P6.18 ON THE NATURE OF HIGHLY DEVIANT SUPERCELL MOTION

Matthew J. Bunkers*
NOAA/NWS Weather Forecast Office, Rapid City, South Dakota

Jon W. Zeitler
NOAA/NWS Houston/Galveston Weather Forecast Office, Dickinson, Texas

1. INTRODUCTION

Knowledge of supercell motion prior to storm formation is critical for short-term forecasting of severe convective weather. The forecast motion can be used to determine the storm-relative helicity (SRH), as well as the storm-relative flow at the middle and upper levels of the supercell, which is important for evaluating its tornadic potential and precipitation distribution (e.g., Rasmussen and Straka 1998; Thompson 1998). Moreover, a correct forecast of supercell motion can lead to better pathcasts of hazardous weather in severe local warnings, especially during the initial stages of the supercell's lifetime.

Previous studies have shown that right- and left-moving supercells move to the right and to the left of the vertical wind shear, respectively (e.g., Weisman and Klemp 1986). Most of the time, supercell motion can be predicted to within 5 m s^{-1} of the observed motion (Bunkers et al. 2000); however, under certain circumstances, the predicted motion may be in error by much greater than 5 m s^{-1}. [The supercells associated with these larger errors are referred to as "highly deviant" in the present paper.] There are several factors which could account for these poor supercell motion estimates (these are discussed further in the results section): (i) use of an unrepresentative sounding; (ii) use of an inappropriate mean wind layer; (iii) exceptionally strong vertical wind shear which can lead to large deviations from the mean wind; (iv) weak mid-level wind shear which can lead to outflow-dominated storms; and (v) external influences, such as orography, storm mergers, and boundary interactions. Items three and four are the focus of the present study.

2. DATA & METHODS

The dataset and methodology to predict supercell motion presented in Bunkers et al. (2000) was used in the present study. Furthermore, 79 additional supercell events were gathered using the methodology they described. In order to forecast supercell motion, their method assumes that the storm moves with the non-pressure-weighted 0–6-km mean wind, and also that the right-moving storm (relative to the vertical wind shear) deviates 7.5 m s^{-1} away from the mean wind and perpendicular to the vertical wind shear. This estimate of supercell motion was used herein as a baseline to compare to the observed supercell motion in an effort to understand the nature of the highly deviant storms.

* *Corresponding author address*: Matthew J. Bunkers, Natl. Wea. Serv., 300 E. Signal Dr., Rapid City, SD 57701-3800; e-mail: matthew.bunkers@noaa.gov.

3. RESULTS

Initially, events were partitioned according to whether the observed supercell motion differed from the forecast supercell motion by either less than or equal to 5 m s^{-1} (dataset #1; hereafter DS1) or greater than 5 m s^{-1} (dataset #2; hereafter DS2). DS1 contained 245 (72%) of the events with a mean absolute error (MAE) between the observed and forecast supercell motion of 2.7 m s^{-1}; and DS2 contained 94 (28%) of the events with a MAE of 7.3 m s^{-1}. The hodographs were composited for each of the two datasets by first translating the 0–0.5-km mean wind to the origin and then rotating the 0–0.5- to 5.5–6.0-km wind shear vector to the x-axis; therefore, the vertical wind shear was concomitant with the x-axis prior to compositing. A comparison of the composite hodographs (Fig. 1a) showed that the shear profile for DS1 (dashed line) was somewhat weaker than that of DS2 (solid line), especially above 3 km. In addition, there was a general tendency for the highly deviant storms in DS2 to move faster ($\mathbf{V_{OBS}}$)—both downshear and to the right of the vertical wind shear—than predicted ($\mathbf{V_{RM}}$).

In an effort to understand the nature of the supercells whose motion deviated significantly from what was predicted (i.e., those in DS2), several additional partitions were constructed. First, previous studies have shown that when the mid- and upper-level wind shear is relatively weak (and hence the storm-relative winds are weak), supercells tend to be outflow-dominated because more precipitation falls near the updraft (e.g., Brooks et al. 1994; Rasmussen and Straka 1998). This often leads to a faster storm motion than what would be anticipated by the baseline method (mentioned above), usually in the downshear direction.

Second, when the vertical wind shear is strong over a sufficiently deep layer (e.g., greater than 35 m s^{-1} measured as the hodograph length over 0–6 km), more ambient horizontal vorticity is available to be tilted into the updraft of the supercell. This can lead to a stronger rotating updraft, and hence to a stronger dynamically forced vertical pressure gradient (Rotunno and Klemp 1985). This suggests that for supercells occurring in environments where the vertical wind shear is large, there is a greater tendency for them to move farther away from the mean wind than for supercells occurring in environments where the vertical wind shear is weak to moderate. Indeed, correlations between the magnitude of the vertical wind shear over various layers

(0–2 through 0–6 km) and the deviation away from the mean wind (perpendicular to the shear) were around 0.20 for the entire 339-supercell dataset. Moreover, the correlations increased to as high as 0.30 (0.40) when only the upper quartile (10 percent) of cases with the strongest vertical wind shear were considered.

As a result of these considerations, DS2 was further subdivided as follows: (i) events which had weak shear throughout both the length of the hodograph (0–8-km shear < 45 m s^{-1}) and in the mid-levels (4–8-km shear < 20 m s^{-1}) were denoted as partition #1 (P1); (ii) events which had strong shear throughout both the length of the hodograph (0–8-km shear > 45 m s^{-1}) and in the mid-levels (4–8-km shear > 20 m s^{-1}) were denoted as partition #2 (P2); and (iii) events which had strong low-level shear (0–3-km > 20 m s^{-1}) and weak mid-level shear (4–8-km < 25 m s^{-1}) were denoted as partition #3 (P3). Furthermore, cases that were documented as low-topped or miniature supercells were discarded because they were often best predicted using the 0–4-km mean wind, and this would have biased the results.

3.1 *Weak 0–8-km Shear Partition*

Only eleven cases met the criteria for P1. The composite hodograph for P1 (Fig. 1b, solid line) had an observed supercell motion ($\mathbf{V_{OBS}}$) that was faster than the predicted motion ($\mathbf{V_{RM}}$) by about 5 m s^{-1} in the downshear direction. This occurred even though the mean wind speed was less for the P1 composite than for the D1 composite, and the D1 composite in Figure 1b (dashed line) had an observed and predicted supercell motion (not shown) that were both between the $\mathbf{V_{RM}}$ and $\mathbf{V_{OBS}}$ positions (i.e., u = 13.0 m s^{-1}, v = -6.5 m s^{-1}). These results are consistent with the weak mid- (5 km) and upper-level (8 km) storm-relative winds (Table 1) that can lead to more precipitation falling near the updraft, and hence a stronger gust front. Modeling results (Weisman and Klemp 1986, their Fig. 15.17F) indicate that this type of hodograph is associated with shorter-lived supercells that eventually become outflow dominated and can evolve into bow echoes. Also note that the shear (0–4- and 0–8-km, Table 1) was near the low end of what is considered favorable for supercell processes to occur. This may explain why the number of cases selected for P1 was the smallest among the three partitions.

3.2 *Strong 0–8-km Shear Partition*

Nineteen cases met the criteria for P2. In contrast to the weak 0–8-km shear partition (P1), the composite hodograph for P2 (Fig. 1c, solid line) had an observed supercell motion ($\mathbf{V_{OBS}}$) that was 6.5 m s^{-1} farther away from the mean wind than predicted ($\mathbf{V_{RM}}$), with no appreciable downshear deviation. Again, this occurred despite the fact that the mean wind speed was much greater for the P2 composite than for any other partition. Thus, this deviation cannot be attributed to advection affects, but more likely was due, at least in part, to updraft–shear interactions. Additionally, since the mid- (4 km) and upper-level (8 km) storm-relative winds were strongest for this partition (Table 1), gust-front lifting was not considered to be a major factor. The SRH was in excess of 400 m^2 s^{-2} for the P2 composite, suggesting the potential for strongly rotating updrafts. The strength of the vertical wind shear and larger deviation away from the mean wind—across the vertical wind shear—is consistent with the theory for supercell dynamics (Weisman and Rotunno 2000).

3.3 *Strong 0–3-km Shear/Weak 4–8-km Shear Partition*

Twenty-three cases met the criteria for P3, which appears to be the most common scenario for highly deviant supercells. The composite hodograph for P3 (Fig. 1d, solid line) had an observed supercell motion ($\mathbf{V_{OBS}}$) that was faster than the predicted motion ($\mathbf{V_{RM}}$) by about 5 m s^{-1}, with similar magnitudes of deviation in both the downshear direction and across the vertical wind shear (i.e., 3.5 m s^{-1}). This can be explained since the P3 composite has certain attributes of both P1 (weak 4–8-km shear) and P2 (strong 0–4-km shear). Like the P1 composite, the mid- (5 km) and upper-level (8 km) storm-relative winds were relatively weak (Table 1); and like the P2 composite, the SRH was in excess of 400 m^2 s^{-2} (Table 1). Therefore, the deviation can be thought of as a combination of updraft–shear interactions and gust-front lifting. Modeling results are generally similar for supercells between the P1 and P3 composites, with the exception that the right-moving member is stronger, more dominant, and longer-lived for the P3 composite (e.g., Weisman and Klemp 1986).

Table 1. Mean statistics for datasets 1-2 and partitions 1-3. Units are m s^{-1} for the shear (SHR) and storm-relative wind (SRW) parameters; the storm-relative helicity (SRH) has units of m^2 s^{-2}. See the results section for the definition of each dataset/partition.

Composite Hodograph	*0–4 SHR*	*4–8 SHR*	*0–8 SHR*	*0–3 SRH*	*5–km SRW*	*8–km SRW*
Dataset #1	21.8	8.9	30.7	191	11	15
Dataset #2	24.6	11.6	36.2	268	10	16
Partition #1	17.8	8.1	25.9	143	6	10
Partition #2	30.1	17.4	47.5	413	17	25
Partition #3	31.8	7.4	39.1	454	10	10

4. FORECAST CONSIDERATIONS

Supercell motion can be effectively anticipated in all but a few cases if one remains cognizant of the processes which control its movement; these can be summarized as follows: (i) advection by a representative mean wind; (ii) propagation away from the mean wind due to updraft–shear interactions; (iii) propagation downshear due to gust-front lifting; and (iv) external factors such as orography and boundaries which can cause erratic movement. The baseline method of Bunkers et al. (2000) encompasses the first two processes, which are considered to be dominant. The third process may be significant 10 to 25 percent of

the time; and it is unknown how often external forces significantly affect supercell motion.

4.1 *Supercell Motion Due to Advection*

Although not specifically addressed in this paper, improper selection of a mean wind can lead to large errors in the forecast motion of supercells. Most of the low-topped and miniature supercells contained in the present dataset were best predicted using a 0–4-km mean wind, and in some cases, a 0–3-km mean wind resulted in the best forecast. These layers represented approximately one-half of the storm's depth. Conversely, a 1–8- or 0–8-km mean wind often produced the best results when the supercells were elevated or their top exceeded 14 km, respectively.

4.2 *Supercell Motion Due to Updraft–shear Interactions*

The current results suggest that when the 0–3- to 0–6-km wind shear becomes strong (i.e., greater than 20 to 35 m s^{-1}, respectively), supercells may deviate much farther away from the mean wind than the 7.5 m s^{-1} suggested by Bunkers et al. (2000) (refer back to Figs. 1c and 1d). The SRH may be well in excess of 400 m^2 s^{-2} in these instances. It is hypothesized that the strong vertical wind shear—and hence the stronger ambient horizontal vorticity—ultimately produces a more vigorous rotating updraft and thus a stronger dynamic vertical pressure gradient force. From the arguments presented in Rotunno and Klemp (1985), this would lead to a larger propagation component perpendicular to the vertical wind shear.

4.3 *Supercell Motion Due to Gust-front Lifting*

Since the motion of 72 percent of the 339 supercell cases in the present dataset can be predicted with a MAE of 2.7 m s^{-1}, gust-front lifting may not always be a significant factor in modulating storm motion. However, during instances when the 4–8-km wind shear, and hence the storm-relative winds, are relatively weak (e.g., Table 1), gust-front lifting may produce an additional component of storm motion which is on the order of 5 m s^{-1} in the downshear direction (e.g., Fig 1b). Thermodynamic considerations such as cloud-base height and boundary-layer humidity (not discussed herein) may modify the extent to which this occurs.

5. CONCLUSIONS

It is hypothesized that for right-moving supercells (i) stronger deep-layer vertical wind shear leads to a stronger mesocyclone, and thus to a greater deviation from the mean wind toward the right of the vertical wind shear; and (ii) weaker mid-level vertical wind shear allows for a stronger cold pool, and thus for a tendency for the supercell to move more rapidly downshear. The latter condition appears to be most common in high-precipitation supercell environments, and has been supported by operational experience (e.g., Brooks et al. 1993; Moller et al. 1994; Conway et al. 1996; Klimowski et al. 1998).

Given this knowledge of the vertical wind shear distribution—as well as the selection of an appropriate mean wind layer—one can make modifications to the initial prediction of supercell motion, minimizing the potential for large errors. It cannot be overemphasized that the hodograph must be viewed from a vertical wind shear perspective in order for these techniques to be successful (see Weisman and Rotunno 2000). The baseline method of Bunkers et al. (2000) can therefore be modified by expecting (i) a larger deviation away from the mean wind during very strong vertical wind shear scenarios; and (ii) a deviation in the downshear direction when the mid-level vertical wind shear is relatively weak. Finally, it should be noted that these are just guidelines, and individual cases will at times differ markedly from the composite (e.g., storms may not always deviate significantly from the baseline motion when in fact the vertical wind shear profile is supportive of it).

5. ACKNOWLEDGMENTS

The authors would like to thank David Carpenter and Bill Read for supporting this work, as well as Brian Klimowski who reviewed the paper.

6. REFERENCES

Brooks, H. E., and C. A. Doswell III, 1993: Extreme winds in high-precipitation supercells. Preprints, *17th Conf. on Severe Local Storms*, St. Louis, MO, Amer. Meteor. Soc., 173-177.

____, ____, and R. B. Wilhelmson, 1994: The role of midtropospheric winds in the evolution and maintenance of low-level mesocyclones. *Mon. Wea. Rev.*, **122**, 126-136.

Bunkers, M. J., B. A. Klimowski, J. W. Zeitler, R. L. Thompson, and M. L. Weisman, 2000: Predicting supercell motion using a new hodograph technique. *Wea. Forecasting*, **15**, 61-79.

Conway, J. W., H. E. Brooks, and K. D. Hondl, 1996: The 17 August 1994 Lahoma, OK supercell: Issues of tornadogenesis and bow echo formation. Preprints, *18th Conf. on Severe Local Storms*, San Francisco, CA, Amer. Meteor. Soc., 52-56.

Klimowski, B. A., M. R. Hjelmfelt, M. J. Bunkers, D. Sedlacek, and L. R. Johnson, 1998: Hailstorm damage observed from the GOES-8 satellite: The 5-6 July 1996 Butte-Meade Storm. *Mon. Wea. Rev.*, **126**, 831-834.

Moller, A. R., C. A. Doswell III, M. P. Foster, and G. R. Woodall, 1994: The operational recognition of supercell thunderstorm environments and storm structures. *Wea. Forecasting*, **9**, 327-347.

Rasmussen, E. N., and J. M. Straka, 1998: Variations in supercell morphology. Part I: Observations of the role of upper-level storm-relative flow. *Mon. Wea. Rev.*, **126**, 2406-2421.

Rotunno, R., and J. B. Klemp, 1985: On the rotation and propagation of simulated supercell thunderstorms. *J. Atmos. Sci.*, **42**, 271-292.

Thompson, R. L., 1998: Eta model storm-relative winds associated with tornadic and nontornadic supercells. *Wea. Forecasting*, **13**, 125-137.

Weisman, M. L., and R. Rotunno, 2000: The use of vertical wind shear versus helicity in interpreting supercell dynamics. *J. Atmos. Sci.*, **57**, 1452–1472.

____, and J. B. Klemp, 1986: Characteristics of isolated convective storms. *Mesoscale Meteorology and Forecasting*, P. S. Ray, Ed., Amer. Meteor. Soc., Boston, 331-358.

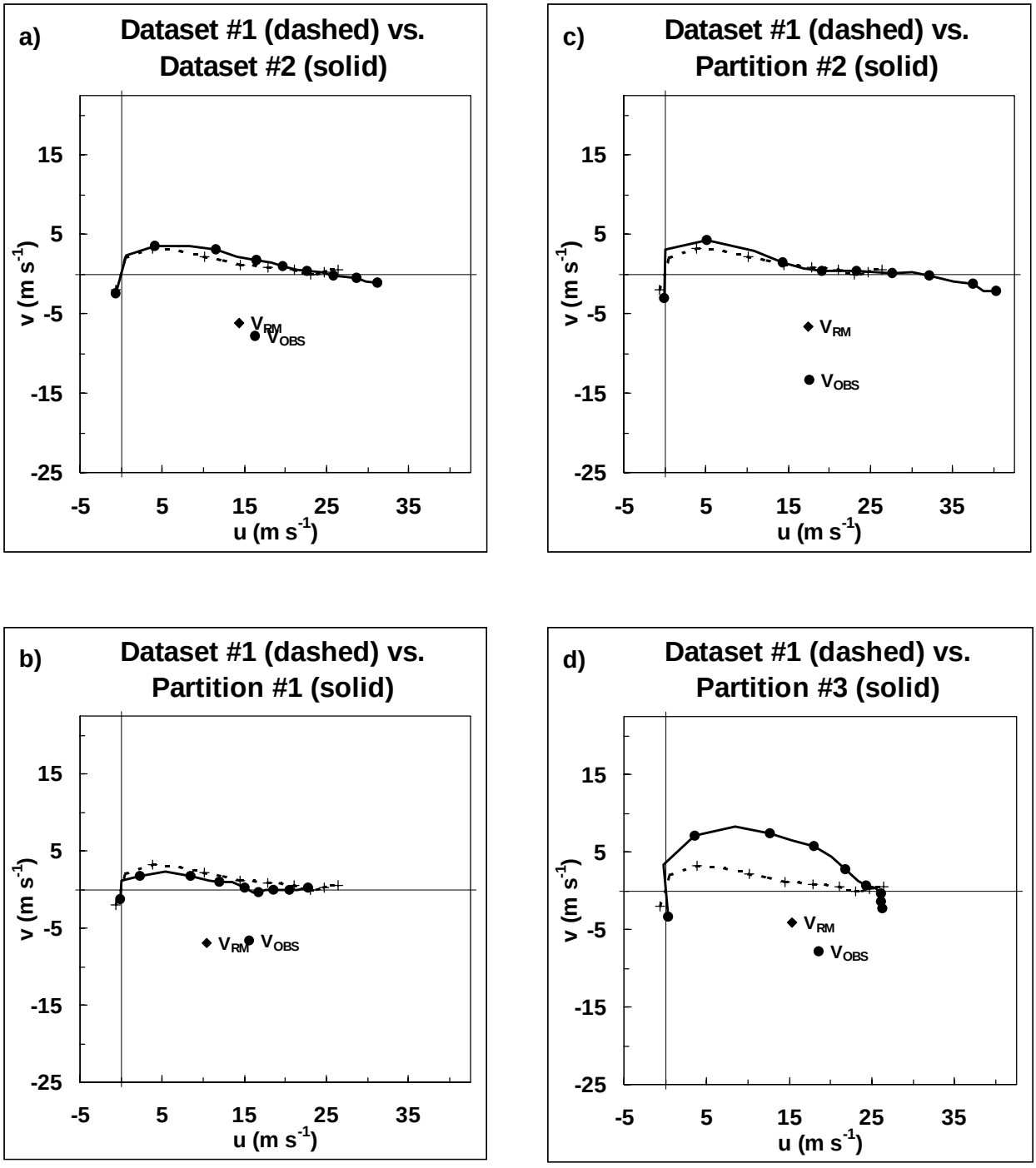

Figure 1. Composite 0–8-km hodographs (m s^{-1}) for: (a) dataset #1 (dashed with plus signs) vs. dataset #2 (solid with circles); (b) dataset #1 (dashed with plus signs) vs. partition #1 (solid with circles); (c) dataset #1 (dashed with plus signs) vs. partition #2 (solid with circles); and (d) dataset #1 (dashed with plus signs) vs. partition #3 (solid with circles). Circles and plus signs are plotted every 1 km above ground level from the surface to 8 km. The composite observed supercell motion for the solid-line hodograph is given as $\mathbf{V_{OBS}}$ (solid circle); the composite baseline prediction of supercell motion for the solid-line hodograph is given as $\mathbf{V_{RM}}$ (diamond). See the results section for the definition of each dataset/partition.